Water Research X 27 (2025) 100299

Contents lists available at ScienceDirect

Water Research X

journal homepage: www.sciencedirect.com/journal/water-research-x

# Smaller sizes of polyethylene terephthalate microplastics mainly stimulate heterotrophic $N_2O$ production in aerobic granular sludge systems

Yingrui Liu [a], Yanying He [a], Qian Lu [a], Tingting Zhu [a], Yufen Wang [a], Yindong Tong [a], Yingxin Zhao [a], Bing-Jie Ni [b], Yiwen Liu [a,*]

[a] School of Environmental Science and Engineering, Tianjin University, Tianjin 300072, PR China
[b] School of Civil and Environmental Engineering, University of New South Wales, Sydney, New South Wales 2052, Australia

ARTICLE INFO

*Keywords:*
Nitrous oxide ($N_2O$)
Microplastics (MPs)
Particle sizes
Aerobic granular sludge (AGS)
Polyethylene terephthalate (PET)

ABSTRACT

Widespread polyethylene terephthalate microplastics (PET MPs) have played unintended role in nitrous oxide ($N_2O$) turnovers (i.e., production and consumption) at wastewater treatment plants (WWTPs). Mainstream aerobic granular sludge (AGS) systems possess potentially strong $N_2O$-sink capability, which may be reduced by PET MPs stress through altering $N_2O$-contributing pathways, electron transfer, and microbial community structures. In this study, the effects of PET MPs with two common particle sizes of effluent from WWTPs (0.1 and 0.5 mm) on $N_2O$ turnovers, production pathways and $N_2O$-sink capability were systematically disclosed in AGS systems by a series of biochemical tests and molecular biological means to achieve the goal of carbon neutrality. The results indicated that 0.1 mm PET MPs could more significantly stimulate $N_2O$ production in AGS systems by inhibiting denitrifying metabolism, compared with control and 0.5 mm PET MPs systems. Specifically, 0.1 mm PET MPs slightly increased the relative abundance of *Nitrosomonas*, reducing $N_2O$ yields via promoting the hydroxylamine ($NH_2OH$) oxidation pathway during nitrification. Also, 0.1 mm PET MPs inhibited the electron transport system activities and the relative abundance of $N_2O$ reductase, hindering $N_2O$ reduction during denitrification. Most importantly, 0.1 mm PET MPs more apparently reduced the $N_2O$-sink capability based on the ratio of $N_2O$ reductase gene and nitrite reductase gene.

## 1. Introduction

Nitrous oxide ($N_2O$), as a potent greenhouse gas with global warming potential of approximately 300 times greater than that of carbon dioxide ($CO_2$) (Tong et al., 2024), potentially contributes to carbon footprints at wastewater treatment plants (WWTPs) (Yu et al. 2022). During the biological nitrogen removal (BNR) process, nitrification and denitrification play a significant role in regulating $N_2O$ emissions at WWTPs (Dai et al. 2021; He et al. 2023a; Su et al. 2023; Zheng et al. 2024). Nitrification contributes to $N_2O$ production by ammonia-oxidizing bacteria (AOB) via two primary pathways including the hydroxylamine ($NH_2OH$) oxidation pathway (He et al. 2023b), i.e., $NH_2OH$→nitrosyl radical (NOH)/nitric oxide (NO)→$N_2O$, and AOB denitrification pathway, i.e., nitrite ($NO_2^-$)→NO→$N_2O$. Denitrification, as a $N_2O$ sink (Conthe et al. 2019), involves four respective specific reductases of heterotrophic denitrifying bacteria (HB), i.e., nitrate ($NO_3^-$), $NO_2^-$, NO, and $N_2O$ reductase (*Nar, Nir, Nor* and *Nos*) for four sequential reductive reactions, i.e., $NO_3^-$→$NO_2^-$→NO→$N_2O$→$N_2$, respectively, through a complete electron transfer chain. Recently, several reports have suggested that aerobic granular sludge (AGS) systems demonstrated lower $N_2O$ emissions compared to conventional activated sludge systems (Liu et al. 2024). However, extreme environmental stress could intensify $N_2O$ emissions in aquatic environments by altering the abundance and activity of related bacteria, enzymes and key genes of AGS in terms of $N_2O$ turnovers (i.e., production and consumption) (Li et al. 2023).

Microplastics (MPs), as an emerging pollutant, have been commonly detected in the influent of the mainstream BNR system in WWTPs (Yang et al. 2019)' (Mahon et al. 2017). Thus, the dominant position of mainstream AGS system for lower $N_2O$ production could be threatened because of MPs stress. Specifically, MPs can alter the biomass (Zheng et al. 2022), extracellular polymeric substance (EPS) contents (Jachimowicz et al. 2022), granule structure (Qin et al. 2020) and microbial abundance (Dai et al. 2020) of AGS as well as the biochemical nitrogen conversion process of the system, all of which are closely

* Corresponding author.
*E-mail address:* yiwen.liu@tju.edu.cn (Y. Liu).

https://doi.org/10.1016/j.wroa.2024.100299
Received 8 November 2024; Received in revised form 16 December 2024; Accepted 27 December 2024
Available online 27 December 2024

related to $N_2O$ turnovers. Recently, He et al. explored the effects of polyethylene terephthalate (PET) MPs (He et al. 2022) and polyvinyl chloride (PVC) MPs (He et al. 2024) with various doses on $N_2O$ emissions during complete nitrogen removal and partial nitrification in activated sludge systems. However, they ignored another important influence characteristic of MPs, particle size (Li et al. 2022; Shi et al. 2024; Zhang et al. 2022). Reportedly, over 90 % of MPs in the effluent of WWTPs were smaller than 0.5 mm and around 60 % of MPs were smaller than 0.1 mm (Mintenig et al. 2017). He et al. (He et al. 2021) studied the inhibition effect of polystyrene MPs (0–0.3 mm) in activated sludge systems on nitrogen conversion, whereas did not further investigate the influence of particle sizes on $N_2O$ emissions. In addition, the interaction between MPs with different particle sizes and granular sludge could alter the structure of AGS and the adhesion by EPS on AGS surfaces (Jachimowicz et al. 2022), which may indirectly affect $N_2O$ emissions. Therefore, systematically exploring the impacts of MPs with different particle sizes on $N_2O$ turnovers in AGS systems could fill the knowledge gaps.

Therefore, this study aimed to reveal the $N_2O$ emissions principle and $N_2O$ turnovers mechanism during nitrification and denitrification in long-term PET MPs-exposed AGS systems by integrating real-time $N_2O$ detecting, related $N_2O$ calculations, isotopic measurements and molecular biological means. This study offered a thorough insight into the influence of PET MPs stress on $N_2O$ turnovers within AGS systems, potentially aiding in assessing the environmental risk of MPs on $N_2O$ footprint at WWTPs in the future.

## 2. Results and discussion

### *2.1. Effects of PET MPs with different particle sizes on $N_2O$ production during a typical cycle and sole nitrification*

The nitrogen removal and $N_2O$ production within three AGS systems were illustrated over a typical 6-h cycle (Fig. 1**A-D**). The results showed that PET MPs stress deteriorated the TN removal efficiency (ca. 0.6 %–15.3 %) and exacerbated $N_2O$ production (ca. 0.13–0.2 %) in AGS systems, especially smaller PET MPs (0.1 mm) exposure (**Text S1**). This was likely because PET MPs could potentially influence $N_2O$ -linked microbial activity through leaching toxic chemicals (i.e., additives) (Seeley et al. 2020) and increasing the generation of reactive oxygen species (2022, Wei et al. 2020).

Fig. 2**A and S3** depicted the nitrogen compounds, DO and pH profiles for the three AGS systems during nitrification batch test 1. The $N_2O$ concentration was gradually produced during 45-min experimental phase. In Fig. 2**B**, $N_2O$ production appeared to decrease in the following order: AGS>AGS_0.5mmPET>AGS_0.1mmPET, i.e., the $N_2O$ production rate (Fig. 2**C**) decreased by 0.01–0.015 mg-N/h/g VSS as the PET MPs exposure ($p < 0.01$), and $N_2O$ emission factors in PET MPs-exposed AGS systems decreased by 0.45–0.56 % (Fig. 2**D**). From Fig. 2**E**, PET MPs stress increased the SP value by ca.1.9–2.3 ‰, confirming that PET MPs (especially smaller PET MPs) altered $N_2O$ production pathways driven by AOB (Fig. 2**H**). Specifically, the AOB denitrification pathway accounted for 54.9 % in the control system (Liu et al. 2024), while the contribution of $NH_2OH$ oxidation pathway gradually increased from 51.6 % to 52.8 % with the decreasing particle sizes of PET MPs. This was likely because MPs might increase the media oxygen content within the nitrifying AGS system (Guo et al. 2024), where oxygen was used for further $NO_2^-$ oxidation to $NO_3^-$ instead of reduction to $N_2O$ through the AOB denitrification pathway, thus leading to the decreasing contribution of AOB denitrification pathway (Liu et al. 2024; Peng et al. 2015).

### *2.2. Impacts of PET MPs with different particle sizes on $N_2O$ turnovers and $N_2O$-sink capability during denitrification*

#### *2.2.1. $N_2O$ turnovers, reduction rates and electron consumption rates*

From Fig. 3**A-C**, compared to the control system, PET MPs (especially

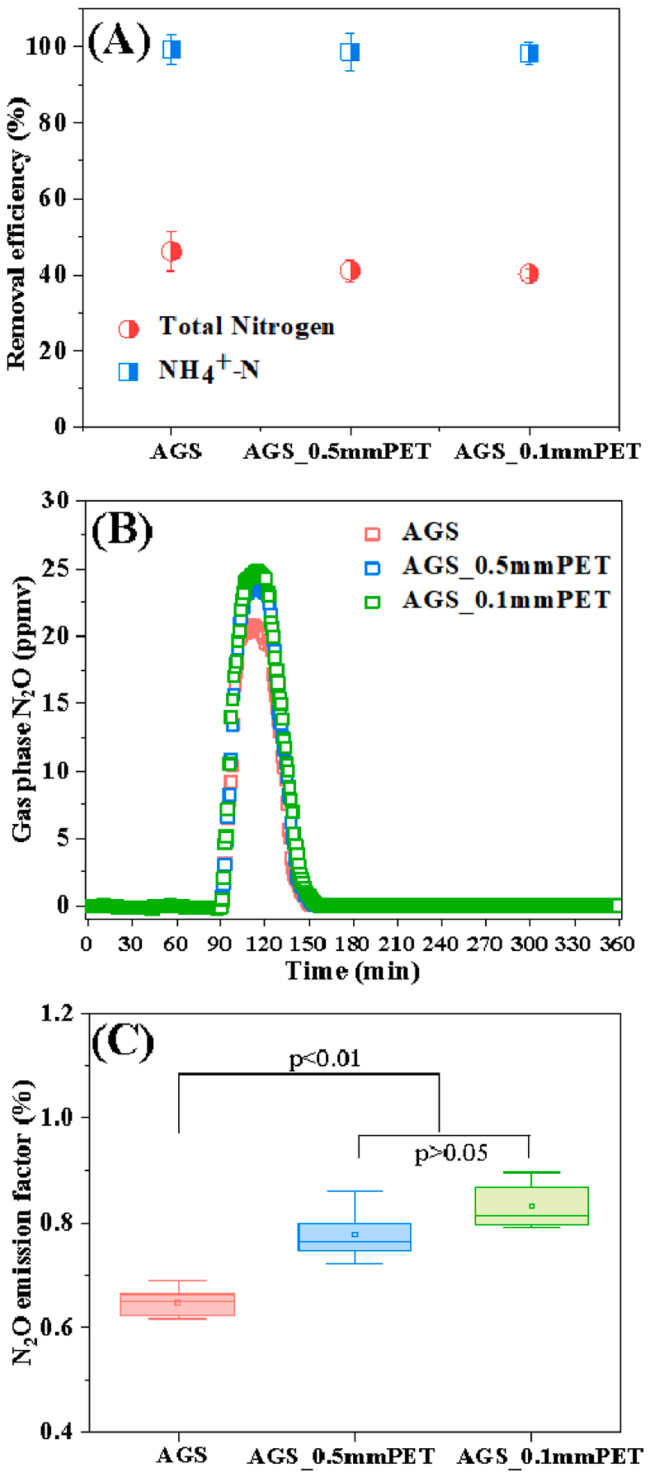


**Fig. 1.** (A) removal efficiency of total nitrogen (TN) and $NH_4^+$-N, (B) gas-phase $N_2O$ and (C) $N_2O$ emission factors in three AGS systems including the control and exposure to two PET MPs particle sizes (i.e., AGS, AGS_0.5mmPET and AGS_0.1mmPET) during a typical 6-h cycle.

0.1 mm PET MPs) stress inhibited $N_2O$ reduction (He et al. 2022) in schemes c and g (i.e., ca.3.82–6.61 mg-N/L) and promoted $N_2O$ accumulation in scheme d (i.e., 0.04–0.2 mg-N/L) during experiment 1 (**Text S2**). Moreover, PET MPs significantly decreased $N_2O$ reduction rates by 2.3–4.8 mg/g VSS/h and electron consumption rates of *Nos* 0.17–0.34 m mole/g VSS/h, and its inhibitory effects was intensified with the decreasing particle sizes from 0.5 to 0.1 mm (Fig. 3**D-I, Text S3**).

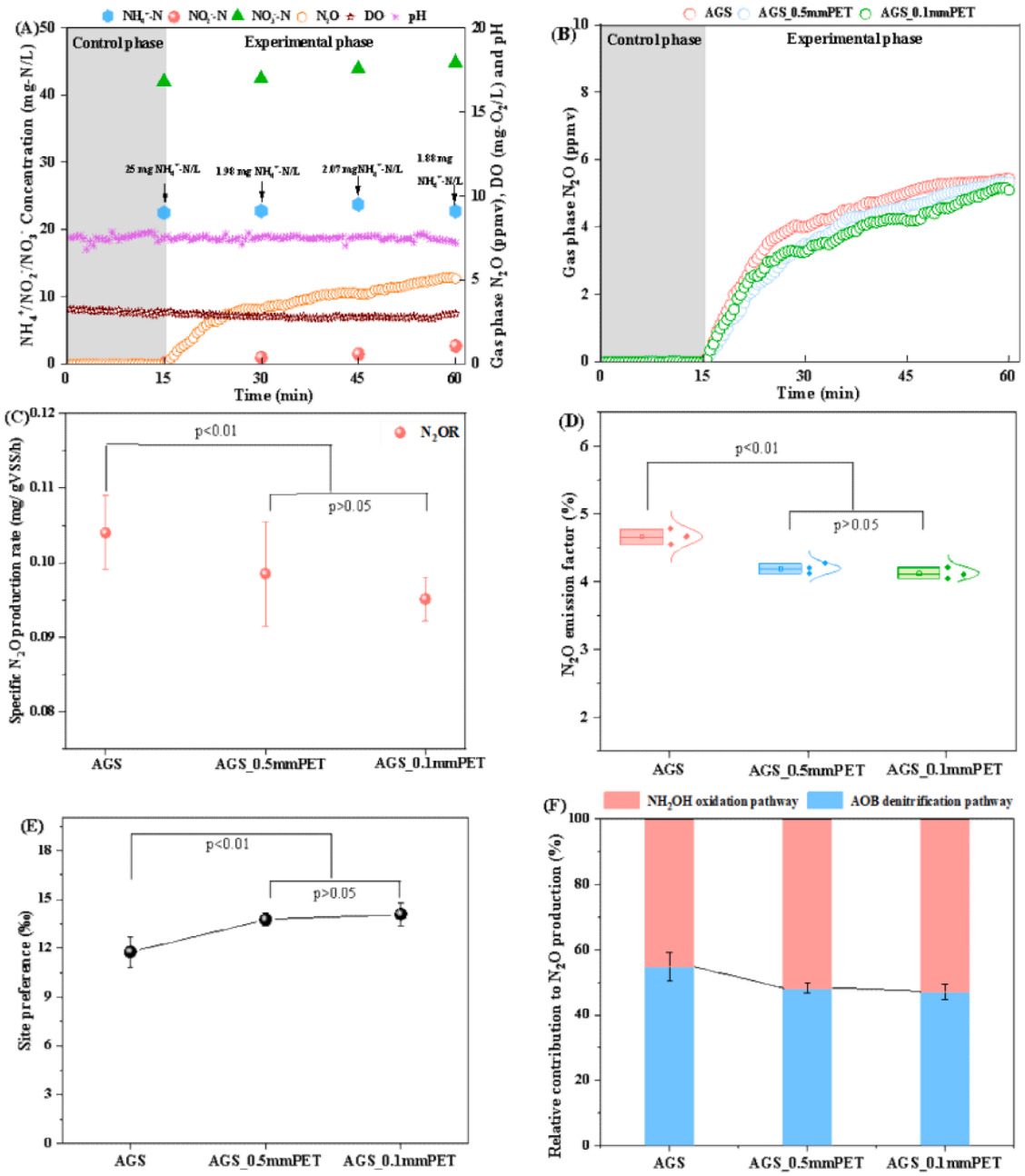


**Fig. 2.** *Batch test 1* during nitrification: (A) $NH_4^+$, $NO_2^-$, $NO_3^-$ DO and $N_2O$ profiles in AGS_0.1mmPET; (B) gas-phase $N_2O$ profiles, (C) $N_2O$ production rate, (D) $N_2O$ emission factors, (E) site preference of $N_2O$ and (F) relative contributions of different $N_2O$ production pathways in AGS, AGS_0.5mmPET and AGS_0.1mmPET.

*2.2.2. Electron competition, distribution, transfer and $N_2O$-sink capability*

In Fig. 4**A**, the susceptibility of $r_{N2O}$ under non-carbon-limiting condition was significantly weakened with PET MPs adding (Pan et al. 2013b), especially in AGS_0.1mmPET (i.e. 6.1 % (e1), 6.2 % (f1) and 13.2 % (g1)). The electron competition intensity under carbon-limiting condition gradually increased (ca. 0.4–0.6) in PET MPs-exposed systems (Fig. 4**A**). In Fig. 4**B**, the average γ (Conthe et al. 2019) decreased from 3.6 in the control system to 3.3 in AGS_0.5mmPET and 3.2 in AGS_0.1mmPET, suggesting an apparent inhibition of PET MPs to $N_2O$-sink capability.

For electron distribution, decreasing electrons distributed to *Nos* with PET MPs exposure were observed in scheme d (Fig. 4**C**), inducing $N_2O$ accumulation described above (Fig. 3**B**) (Pan et al. 2013a). The highest decreasing rates of electron distributed to *Nos* in schemes e (Fig. 4**D**), f (Fig. 4**E**) and g (Fig. 4**F**) were observed in AGS_0.1mmPET. Most typically, in scheme g, electrons allocated to *Nos* in AGS_0.1mmPET reduced by 8.5–10.5 % compared to that of the control system (Fig. 4**F**). Such observations were possibly due to the inhibitory influence of PET MPs on bioenergy conversion (**Text S4**) (Almeida et al. 1995; Oberoi et al. 2021), electron transfer and the activity of several key enzymes.

Reduced nicotinamide adenine dinucleotide (NADH) was mainly involved in the front-end electron transfer process (Chen and Strous 2013; Sazanov and Hinchliffe 2006). In Fig. 4**G**, the NADH concentration of 187.3 ng/L in the control system obviously decreased to 175.6 ng/L in AGS_0.5mmPET, and further declined to 134.2 ng/L in AGS_0.1mmPET, indicating an inhibitory effect of PET MPs on the front-end electron transfer process. Periplasmic cytochrome c (Cyt-c), as an electron carrier, directly provided electrons to *Nir* and *Nos* in the downstream electron pool (Qi et al. 2012). In Fig. 4**H**, after exposure to 0.5 and 0.1 mm PET MPs, the Cyt-c concentration decreased by 2.77 and 6.44 nmol/L, respectively, compared to the control. The results

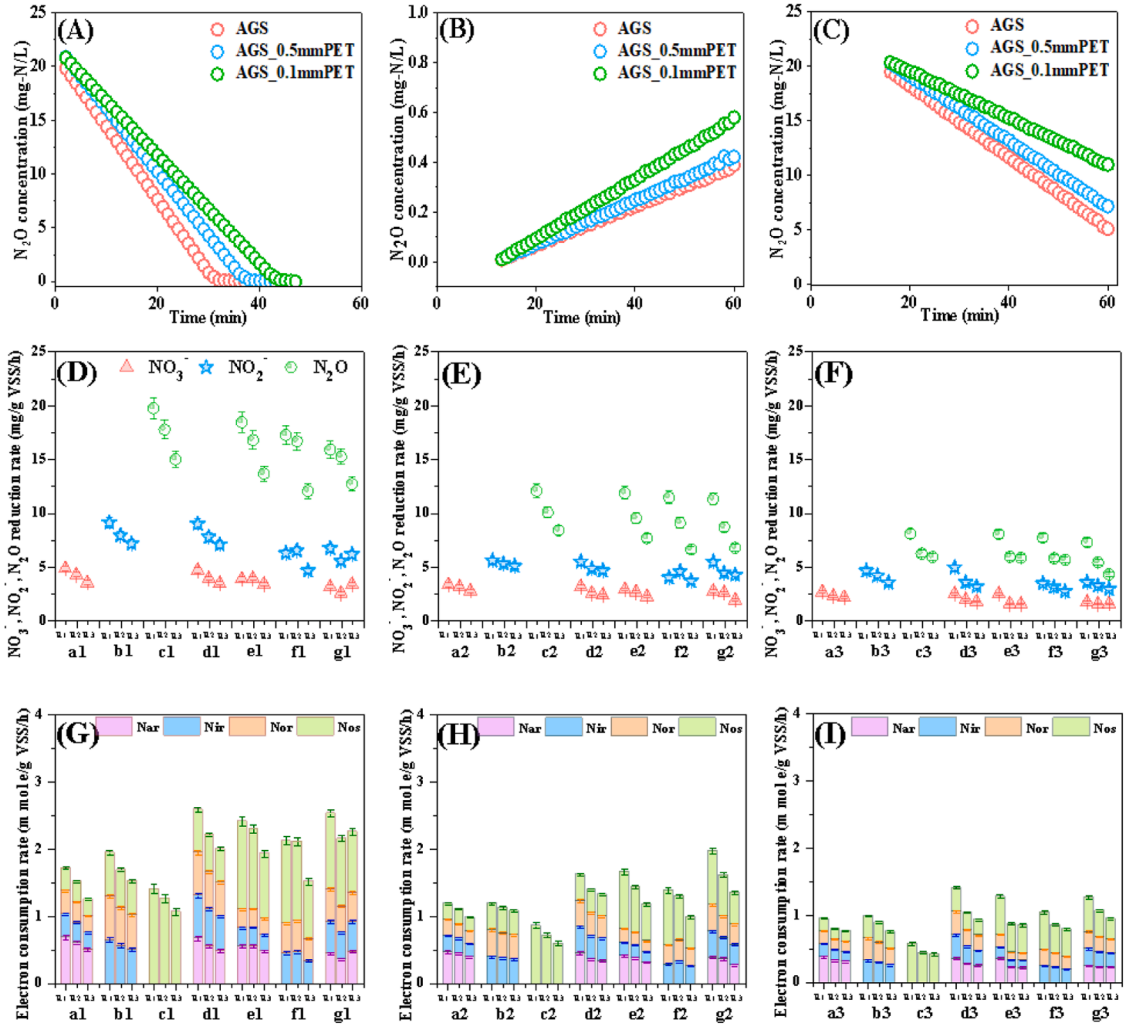


**Fig. 3.** *Batch test 2* during denitrification in AGS (R1), AGS_0.5mmPET (R2) and AGS_0.1mmPET (R3): liquid-phase $N_2O$ profiles from *experiment 1* of three AGS systems in *scheme* (A) *c*, (B) d and (C) g. $NO_x$ reduction rate and electron consumption rate in *schemes a*-g under non-carbon-limiting conditions during (D and G) *experiment 1*, and under carbon-limiting conditions during (E and H) *experiment 2* and (F and I) *experiment 3*.

indicated that PET MPs inhibited the activity of electron carriers (i.e., Cyt-c) in the downstream electron pool, further reducing the number of electrons distributed to *Nos*. From Fig. 4**I** that electron transport system activity (ETSA) of 1.39 mg TF/g VSS/h in the control decreased to 1.24 mg TF/g VSS/h in AGS_0.5mmPET and 1.19 mg TF/g VSS/h in AGS_0.1mmPET. This delineated that PET MPs significantly hindered electron transfer efficiency in the AGS system.

### *2.3. Effects of PET MPs with different particle sizes on microbial community and functional gene abundance*

The rarefaction curves and alpha diversity for three samples (i.e., in two PET-exposed groups were higher than the control group) indicated that PET MPs could enhance microbial richness and diversity in AGS systems ((**Fig. S4–5**). At the phylum level (Fig. 5**A**), an increasing relative abundance of *Bacteroidota* (ca. 3.3–9.5 %) was observed in PET MPs-exposed systems (Dai et al. 2020; He et al. 2022; Wang et al. 2023; Zhang et al. 2017). In addition, the highest relative abundance of *Bacteroidota* (27.5 %) was observed in AGS_0.1mmPET, indicating that smaller PET MPs were more easily adhered to AGS surfaces (Wang et al. 2021). At the genus level (Fig. 5**B**), *Thauera* was plausibly associated with $N_2O$ reduction activity during the complete denitrification (Chourey et al. 2013) and its abundance was decreased by 4.5 % in AGS_0.1mmPET. Also, *Rhodobacter* was documented to be associated with $N_2O$ emission and the expression of the *nirK* gene (Vieira et al. 2019). The decreasing relative abundance of *Rhodobacter* (i.e., decreased by 0.16 % in AGS_0.1mmPET) could induce $NO_2^-$ accumulation, and then lead to $N_2O$ accumulation. Moreover, the relative abundance of *Nitrosomonas* (i.e., AOB) increased from 0.8 % in the control system to 1.1 % in AGS_0.1mmPET (He et al. 2022).

Phylogenetic Investigation of Communities by Reconstruction of Unobserved States (PICRUSt2) and Kyoto Encyclopedia of Genes and Genomes (KEGG) database were utilized to explore the relative abundance of crucial genes and enzymes associated with $N_2O$ production and reduction (He et al. 2022). From Fig. 5**C** and **Table S1**, ammonia mono-oxygenase (*AMO*), represented by EC 1.14.99.39 (K10944, K10945 and K10946), was slightly elevated by 0.2 % in AGS_0.1mmPET, consistent with the variation of *Nitrosomonas*. The relative abundance of hydroxylamine oxidoreductase (*HAO)* represented by EC 1.7.2.6 (K10535) also increased in AGS_0.1mmPET, further explaining the increasing contribution of $NH_2OH$ oxidation pathway (Fig. 2**F**). The relative abundance of all four denitrification reductases (i.e., *Nap/Nar, Nir, Nor* and *Nos*) showed a decreasing trend in AGS_0.1mmPET (Fig. 5**C-D**). For example, the abundance of *Nos* (K00376) decreased from 2.2 % in the control system to 2.1 % in AGS_0.5mmPET and 1.8 % in AGS_0.1mmPET, further confirming the inhibitory effect of PET MPs (especially 0.1 mm) on $N_2O$ reduction. For quantitative polymerase chain reaction (qPCR), the abundance of *NosZ* in AGS_0.5mmPET and

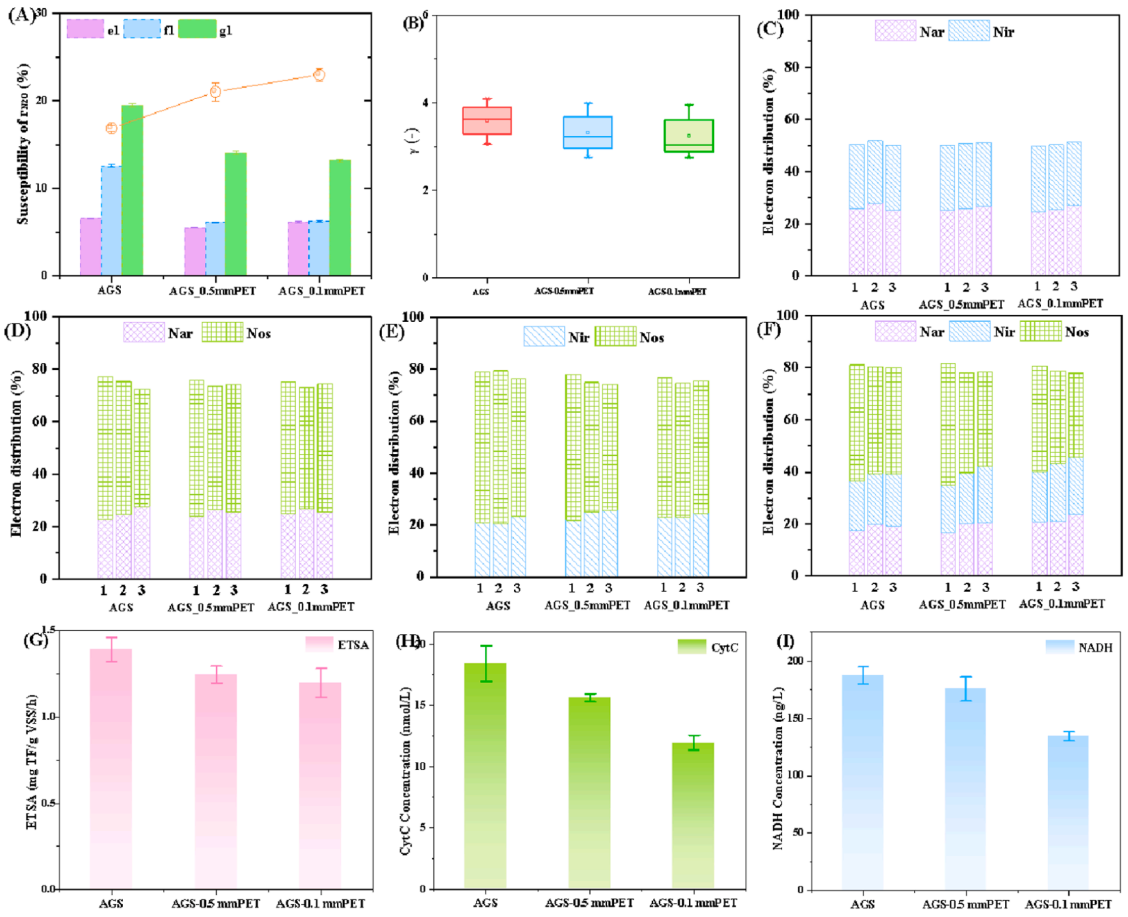


**Fig. 4.** *Batch test 2* during denitrification in AGS, AGS_0.5mmPET and AGS_0.1mmPET: (A) degree of decrease in $N_2O$ reduction rates ($r_{N2O}$) from *experiment 1* and the intensity of electron competition during *experiment 1–3*; (B) $N_2O$-sink capability represented by the ratio γ; percentages of electrons distribution in *scheme* d (C), *e* (D), *f* (E), g (F) for *experiments 1, 2 and 3*, respectively. (G) ETSA, (H) Cyt-c and (I) NADH concentrations.

AGS_0.1mmPET was reduced by 13.6 % and 27.3 %, respectively (**Table S2**). The reduced abundance of *Nir* (ca. 11.2 %−13.8 % under PET MPs stress) was regarded as mainly ascribed to HB. Additionally, decreased *NosZ*/(*NirS*+*NirK*) (Fig. 5**E**) was observed in PET MPs-exposed systems (especially 0.1 mm), suggesting that PET MPs exposure weakened the $N_2O$-sink capacity in AGS systems (Chen et al. 2020).

### 2.4. Mechanism of PET MPs with different particle sizes influencing $N_2O$ emissions in AGS systems

During a typical cycle, PET MPs (especially smaller particle sizes) inhibited total nitrogen removal (Fig. 1**A**) and stimulated $N_2O$ production (Fig. 1**C**) in AGS systems. For nitrification, PET MPs exposure faintly increased the relative abundance of *Nitrosomonas* and *AMO/HAO* (Fig. 5**B-D** and **Table S1**), thus slightly reducing $N_2O$ yields produced by AOB (Fig. 2**D**) in the AGS system via promoting the contribution of the $NH_2OH$ oxidation pathway (Fig. 2**F**). Therefore, the upward trend and the downward trend of $N_2O$ emission factors in cyclic and nitrification batch tests, respectively (Fig. 1**C** and 2**D**), indicated that PET MPs stimulated the total $N_2O$ production in AGS systems mainly by inhibiting the denitrification process. For denitrification, PET MPs (especially smaller particle sizes) inhibited the activity of NADH (Fig. 4**I**) and Cyt-c (Fig. 4**H**) to reduce the electron transport activity (Fig. 4**G**), reduced electron affinity of *Nos* and intensified the electron competition intensity, thus inducing $N_2O$ accumulation. In addition, PET MPs reduced the distribution of electrons to *Nos*, thereby hindering $N_2O$ reduction (Fig. 3**D**). Subsequently, PET MPs reduced the relative abundance of denitrifiers and enzymes, especially key genes associated with $N_2O$ turnovers (*NirK, NirS, NosZ*), restraining the $N_2O$-sink capability during denitrification in AGS systems (Fig. 4**B,** 5**E**).

Smaller PET MPs (0.1 mm) would more stimulate $N_2O$ emission and inhibited $N_2O$ reduction. Specifically, PET MPs first increased the relative abundance of *Bacteroidota* conducive to their adhesion to AGS surfaces (Fig. 5**A**), laying the foundation for the interaction between PET MPs and AGS. The surface of AGS observed by SEM collected from the control system was dense and complete (**Fig. S6A**), while that exposed to PET MPs was damaged and had many cracks (**Fig. S6B-C**). Previous studies have reported that microplastics could attach to the surface of AGS (Wang et al. 2021), which prevented the transfer of nutrient matrix, resulting in a decrease of EPS content secreted by AGS (Zhang et al. 2020). The result of EPS further indicated that smaller PET MPs would be easier to accumulate in large quantities on AGS (**Fig. S7**). Therefore, smaller PET MPs (0.1 mm) should be given attention in $N_2O$ emissions during nitrogen removal in AGS systems, because after all, 60 % of MPs smaller than 0.1 mm in the effluent of WWTPs were still detected.

### 2.5. Implications

This work exhibited that smaller PET MPs significantly stimulated $N_2O$ production via inhibiting denitrification in the AGS system. The effect of different concentrations of MPs on $N_2O$ production in wastewater treatment has been preliminatively understood (He et al. 2022; Li et al. 2020), while the influence of MPs structural morphology (e.g., particle sizes) is still unknown. This work explored whether $N_2O$ turnovers were promoted or inhibited by PET MPs with different particle

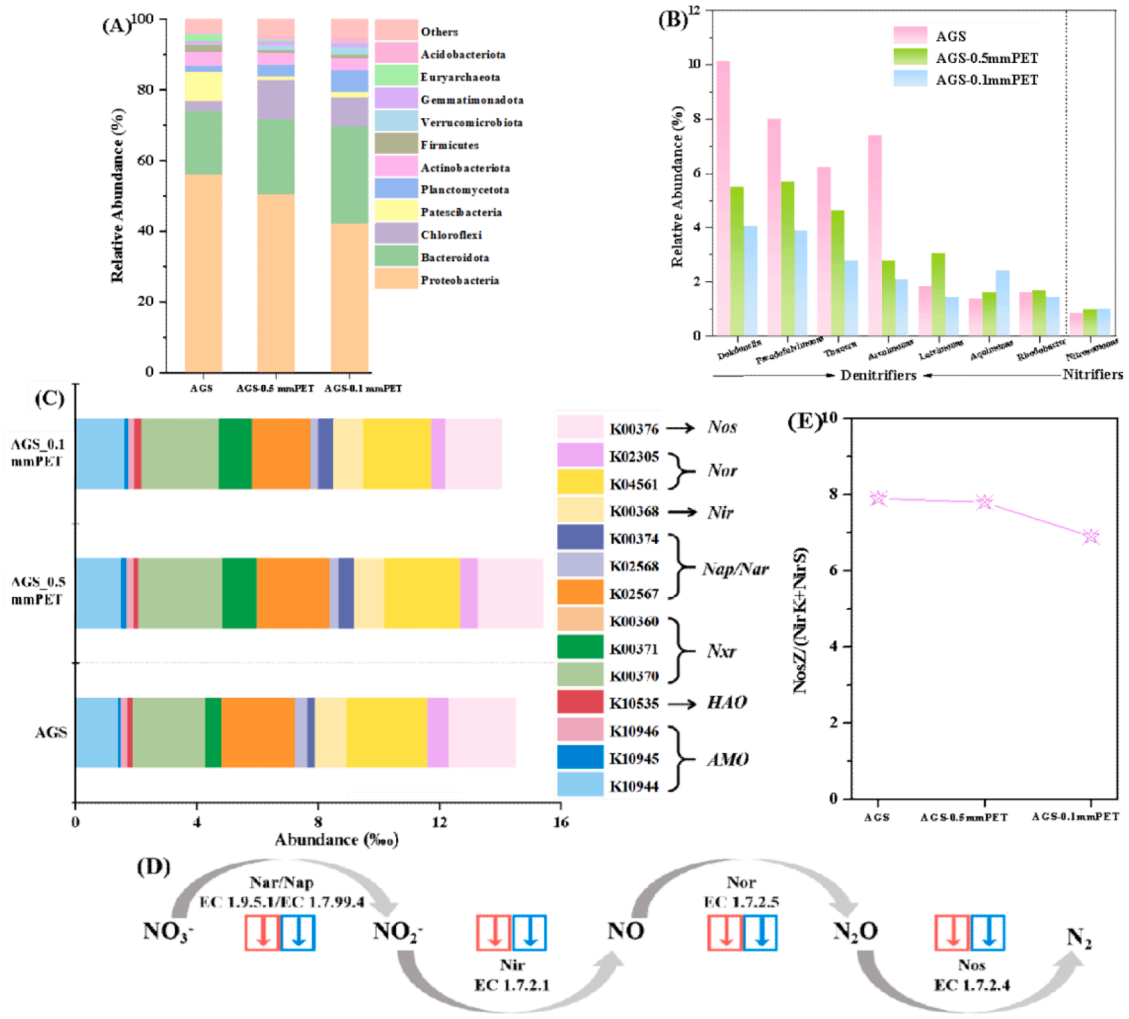


**Fig. 5.** Relative abundance of bacterial populations in AGS, AGS_0.5mmPET and AGS_0.1mmPET: (A) at phylum level, (B) at genus level, (C) the predicted relative abundances of key enzymes, (D) the nitrogen metabolism KEGG pathway related to $N_2O$ turnovers and (E) ratio of *nosZ* and *nirK*+*nirS* from qPCR.

sizes during nitrification and denitrification in AGS systems, ultimately identifying particle sizes and underlying mechanisms that stimulated higher $N_2O$ emissions. Specifically, the relative abundance of denitrifiers and reductase activity in AGS are inhibited by PET MPs (especially 0.1 mm). Flocs could promote $N_2O$ reduction during denitrification (Liu et al. 2023c), thus the lack of denitrifiers in AGS can be compensated by the addition of returned floc sludge to establish the suspend/attach-based system. In addition, PET MPs (especially smaller sizes) also inhibit the electron transport chain. As the main source of electron donors during denitrification in the AGS system, extra organic carbon may help to alleviate the negative effect of PET MPs on $N_2O$ turnovers. Additionally, over 90 % of MPs in the effluent were smaller than 0.5 mm (around 60 % of MPs were smaller than 0.1 mm) at WWTPs (Mintenig et al. 2017; Zhang et al. 2024a; Ziajahromi et al. 2017). Therefore, a finer screen or diverter can be set before entering the AGS system to avoid AGS treating wastewater containing smaller MPs and further alleviate $N_2O$ footprint in AGS systems.

## 3. Conclusions

This work aimed to uncover effects and mechanisms of PET MPs with different particle sizes on $N_2O$ turnovers in mainstream AGS systems. 0.1 mm PET MPs further exacerbated $N_2O$ emissions by 8.2 % compared to 0.5 mm PET MPs during cyclic studies. PET MPs slightly reduced $N_2O$ production by weakening the contribution of the AOB denitrification pathway (by 11.8 %−14 %). PET MPs inhibited the electron transfer activity, thus hindering $N_2O$ reduction and inducing $N_2O$ accumulation during denitrification in AGS systems. Also, PET MPs (especially 0.1 mm) reduced the relative abundance of *nirK, nirS, nosZ*, restraining the $N_2O$-sink capability during denitrification in AGS systems. Therefore, this study provided a theoretical basis for the effect of MPs with different particle sizes on $N_2O$ emissions at WWTPs, and various particle sizes of MPs are worth studying in the future.

## 4. Materials and methods

### 4.1. Experimental granules, PET MPs, setup and cyclic study

The inoculated AGS with granule size of ca. 1.0 mm was obtained from a lab-scale mother AGS sequencing batch reactor (AGS-SBR) fed with synthetic wastewater (**Table S3**). The PET MPs with two particle sizes (i.e., 0.5 and 0.1 mm) were obtained from HuaChuang Co., Ltd. (Dongguan, China). Two experimental AGS-SBRs fed with 0.5 and 0.1 mm PET MPs (5 mg/L) named AGS_0.5mmPET and AGS_0.1mmPET, and a control AGS-SBR (0 mg/L of PET MPs) were operated for over 120 days in this study. (**Text S5**). A typical 6 h cyclic test was complemented on day 120 to evaluate $N_2O$ emissions in each AGS-SBR (**Text S6**).

### 4.2. Batch tests design

#### 4.2.1. $N_2O$ heterotrophic consumption tests

To verify no $N_2O$ turnovers by heterotrophs during nitrification batch tests, three essential $N_2O$ heterotrophic consumption tests by heterotrophic bacteria under aerobic conditions without organic carbon were carried out. In order to eliminate the interference of endogenous denitrification, the 1-h experiment was selected to uncover $N_2O$ production mechanism by AOB. These consumption tests utilized the same liquor as described above and were performed at DO levels of 3.0 mg-$O_2$/L. The tests were conducted in a full-sealed reactor at 25 ± 1 °C, eliminating the headspace. Each test contained evenly mixed aerobic granules. Once the appointed DO concentration was reached, the aeration was stopped immediately. Afterward, the freshly prepared saturated $N_2O$ solution was transferred to the reactor to obtain an $N_2O$ concentration of 1.1 mg-N/L. Fig. S1 showed that the concentration of DO was almost stable within 1 h, since no additional organic carbon, $NH_4^+$, or $NaHCO_3$ was added.

#### 4.2.2. Batch tests during nitrification

For nitrification (batch test 1), batch tests were conducted to investigate $N_2O$ production and its pathways by AOB under different particle sizes of PET MPs stress at 25 mg-N/L $NH_4^+$, 3.0 mg-$O_2$/L of dissolved oxygen (DO) and pH=7.5 (**Table S4**). All batch tests were conducted after the $N_2O$ heterotrophic consumption test (Section 4.2.1), to exclude the interference of heterotrophic bacteria (**Fig. S1**). The batch reactor operation, granules and samples extraction, DO and pH control, as well as the selection of experiment duration and phase were all consistent with our previous study[]. Aerobic granules were individually extracted from the three reactors during the decanting period and washed six times. Each batch test was conducted in a reactor with a working volume of 800 mL and a sealable lid. DO and pH (adjusted by 1 M HCl or $NaHCO_3$) was dynamically maintained through a programmed logic controller (PLC), and monitored online using a DO probe (MIK-DO-7012–7 M) and a pH probe (MIK-pH-5018-BBL5), respectively. Mixed liquor volatile suspended solids (MLVSS) from the end of each batch test were measured in triplicate. $NH_4^+$ and DO levels were controlled to be relatively stable during the entire experiment, which were separately achieved through the ammonia oxidation rate (AOR) calculation based on a $K_La$ test (**Text S7**), and two air/$N_2$ mass flow controllers (AST10-DLCMX, Asert, **Text S8**). The total gas flow rate, regulated by these controllers, was consistently maintained at 0.5 L/min. Each batch test had a duration of 60 min. The first 15 min (i.e., the control phase) were conducted to ensure that any observed $N_2O$ production originated exclusively from heterotrophic denitrification bacteria. During the subsequent 45 min (i.e., the experimental phase), a solution containing 39.43 g/L of $NH_4Cl$ and 83.3 g/L of $NaHCO_3$ was added to achieve an initial $NH_4^+$ concentration of approximately 25 ± 4 mg-N/L, along with adequate $HCO_3^-$. Sample collection for the analysis of $NH_4^+$, $NO_2^-$, and $NO_3^-$ concentrations occurred every 15 min. The gas-phase $N_2O$ levels were monitored online by a $N_2O$ analyzer (AO2020 series, ABB, **Text S9**).

#### 4.2.3. Batch tests during denitrification

Batch tests during denitrification with the addition schemes of nitrogen compounds including seven combinations of $NO_3^-$, $NO_2^-$ and $N_2O$ (schemes a, b, c, d, e, f, g) under conditions of sufficient and insufficient carbon sources were designed in **Table S5**. All batch tests were performed using glucose/sodium acetate as the electron donor. The initial $NO_3^-$, $NO_2^-$ and $N_2O$ concentrations of ca. 20 mg-N/L were achieved by injecting $NaNO_3$, $NaNO_2$ or $N_2O$ stock solution, respectively. For the non-carbon-limiting condition (experiment 1), the COD stock solution (glucose/sodium acetate=1/3) was added to obtain an initial COD/N ratio of 10. Separately, schemes a, b and c in experiment 1 were compared to evaluate the maximum specific reduction rates of $NO_3^-$, $NO_2^-$ and $N_2O$ for the three PET MPs-exposed AGS systems. Individually, schemes d and g in experiment 1 were compared to assess varying $N_2O$ accumulation and reduction in the presence of multiple nitrogen oxide ($NO_x$, i.e., suitable for the actual wastewater treatment) for the three AGS systems. For the carbon-limiting condition, the COD stock solution was added to the batch reactor through a peristaltic pump with a slow feeding mode to achieve a carbon loading rate of 60 mg-COD/g VSS/h in experiment 2 and 20 mg-COD/g VSS/h in experiment 3. Such design was aimed to explore the $NO_x$ reduction rates, $N_2O$ reduction capability, electron competition and electron distribution for the three AGS systems. The batch reactor operation, granules and samples extraction, pH control and $N_2O$ stock solution acquisition were demonstrated in detailed in **Text S10**. The liquid-phase $N_2O$ concentrations were measured continuously by an Unisense microsensor ($N_2O$-R-100, Unisense A/S, **Text S9**).

### 4.3. Calculations

During nitrification batch tests, the specific $N_2O$ production rate (mg-N/g VSS/h) was computed by dividing the gaseous $N_2O$ concentration by the MLVSS concentration of AGS, and then multiplying by the gas flow rate. The average $N_2O$ production rate was determined by calculating the average during the period with stable values of $N_2O$ production rate (relatively constant in all cases). The $N_2O$ emission factor was calculated as the ratio of emitted $N_2O$—N to converted $NH_4^+$-N. The converted $NH_4^+$-N concentration was determined based on the added and measured $NH_4^+$-N profiles according to our previous study (Liu et al. 2024). The calculations of the SP-based quantification of two $N_2O$ production pathways during nitrification are presented in **Text S11**.

During denitrification batch tests, the maximum $NO_3^-$, $NO_2^-$ and $N_2O$ consumption rates were calculated via linear regression of $NO_3^-$, $NO_2^-$ and $N_2O$ profiles, respectively. Such rates were divided by the MLVSS concentration to obtain the specific reduction rates. The calculation of $NO_x$ reduction rate, electron consumption rate and electron distribution were demonstrated in **Text S12**. Susceptibility of $r_{N2O}$ and the intensity of electron competition were calculated according to previous studies (He et al. 2024).

$NO_3^-$ reduction rates in the presence of sole $NO_3^-$ scheme ($r_{NO3}$) and $N_2O$ reduction rates under the absence of other nitrogen compounds ($r_{N2O}$) were regarded as estimates of the maximum $N_2O$ production rates ($VmaxNO_3^-\rightarrow N_2O$=V1) and the maximum $N_2O$ reduction rates ($VmaxN_2O\rightarrow N_2$=V2), respectively, assuming no obvious intermediates accumulation. The ratio $\gamma$ = V2/V1 was calculated to express the $N_2O$-sink capacity of AGS (Conthe et al. 2019). Additionally, the $N_2O$-sink capacity was also represented by the ratio of *nosZ* and *Nir* (i.e., *nirK*+*nirS*) from quantitative PCR (He et al. 2024).

### 4.4. Analytical methods

$NH_4^+$, $NO_2^-$, $NO_3^-$, MLVSS, and MLSS measurements were carried out using standard methods (Association and Washington 1995). Surface morphologies of MPs and sludge were examined utilizing scanning electron microscopy (SEM, Hitachi S4800, Japan) (Wang et al. 2024b). The EPS extraction and component determination were according to a previous study (Liu et al. 2023b; Wang et al. 2024a; Zhang et al. 2024b). The electron transport system activity (ETSA) at the end of the typical cycle in each AGS-SBR was determined by using 2, 3, 5-triphenyltetrazolium chloride (**Text S13**) (Guo et al. 2023; Guo et al. 2022). Enzyme-linked biological nicotinamide adenine dinucleotide (NADH) kit was used to determine the NADH content in AGS-based samples (Xi et al. 2013). The periplasmic Cyt-c was collected by centrifugating (8000 rpm, 5 min) the effluent from the end of typical cycle in each AGS system, subsequently measured using an UV–VIS spectrophotometer at 520 nm (Liu et al. 2023a). High-throughput sequencing was employed to discern variations in the microbial community following PET MPs exposure. The real-time PCR amplification was conducted using

universal primers 515F and 806R targeting the V4 region of bacterial 16S DNA genes (Xiang et al. 2023). Functional gene abundances were assessed by quantitative PCR with the primers detailed in **Table S6** (Han et al. 2022; Zheng et al. 2023). Data analysis was performed using SPSS 26.0 (Wang et al., 2022), and statistical significance was considered for $p < 0.05$ (Tian et al. 2022).

## CRediT authorship contribution statement

**Yingrui Liu:** Writing – original draft. **Yanying He:** Conceptualization. **Qian Lu:** Data curation. **Tingting Zhu:** Formal analysis. **Yufen Wang:** Investigation. **Yindong Tong:** Methodology. **Yingxin Zhao:** Project administration. **Bing-Jie Ni:** Validation. **Yiwen Liu:** Writing – review & editing.

## Declaration of competing interest

The authors declare that they have no known competing financial interests or personal relationships that could have appeared to influence the work reported in this paper.

## Acknowledgements

This study was funded by National Natural Science Foundation of China through projects (No. 52470108). The authors are grateful to the research collaboration.

## Supplementary materials

Supplementary material associated with this article can be found, in the online version, at doi:10.1016/j.wroa.2024.100299.

## Data availability

Data will be made available on request

## References

Almeida, J.S., Reis, M.A.M., Carrondo, M.J.T., 1995. Competition between nitrate and nitrite reduction in denitrification by Pseudomonas fluorescens. Biotechnol. Bioeng.
Association, C., Washington, D., 1995. APHA, A. P. H. A.: standard methods for the examination of water and wastewater. Am. Phys. Educ. Review 24 (9), 481–486.
Chen, H., Zeng, L., Wang, D., Zhou, Y., Yang, X., 2020. Recent advances in nitrous oxide production and mitigation in wastewater treatment. Water Res. 184, 116168.
Chen, J., Strous, M., 2013. Denitrification and aerobic respiration, hybrid electron transport chains and co-evolution. Biochimica et Biophysica Acta (BBA) - Bioenerg. 1827 (2), 136–144.
Chourey, K., Nissen, S., Vishnivetskaya, T., Shah, M., Pfiffner, S., Hettich, R.L., LöFfler, F. E.J.P., 2013. Environmental proteomics reveals early microbial community responses to biostimulation at a uranium- and nitrate-contaminated site. Proteomics 13 (18–19), 2921–2930.
Conthe, M., Lycus, P., Arntzen, M.Ø., Ramos da Silva, A., Frostegård, Å., Bakken, L.R., Kleerebezem, R., van Loosdrecht, M.C.M., 2019. Denitrification as an N2O sink. Water Res. 151, 381–387.
Dai, H.-H., Gao, J.-F., Wang, Z.-Q., Zhao, Y.-F., Zhang, D., 2020. Behavior of nitrogen, phosphorus and antibiotic resistance genes under polyvinyl chloride microplastics pressures in an aerobic granular sludge system. J. Clean. Prod. 256, 120402.
Dai, H., Han, T., Sun, T., Zhu, H., Wang, X., Lu, X., 2021. Nitrous oxide emission during denitrifying phosphorus removal process: a review on the mechanisms and influencing factors. J. Environ. Manage. 278, 111561.
Guo, H., Tian, L., Liu, S., Wang, Y., Hou, J., Zhu, T., Liu, Y., 2023. The potent effects of polyoxometalates (POMs) on controlling sulfide and methane production from sewers. Chem. Engineer. J. 453, 139955.
Guo, T., Lu, C., Chen, Z., Song, Y., Li, H., Han, Y., Hou, Y., Zhong, Y., Guo, J., 2022. Bioinspired facilitation of intrinsically conductive polymers: mediating intra/extracellular electron transfer and microbial metabolism in denitrification. Chemosphere 295, 133865.
Guo, T., Pan, K., Chen, Y., Tian, Y., Deng, J., Li, J., 2024. When aerobic granular sludge faces emerging contaminants: a review. Sci. Total Environ. 907, 167792.
Han, F., Zhang, M., Liu, Z., Han, Y., Li, Q., Zhou, W., 2022. Enhancing robustness of halophilic aerobic granule sludge by granular activated carbon at decreasing temperature. Chemosphere 292, 133507.
He, Y., Li, L., Song, K., Liu, Q., Li, Z., Xie, F., Zhao, X., 2021. Effect of microplastic particle size to the nutrients removal in activated sludge system. Mar. Pollut. Bull. 163, 111972.
He, Y., Li, Y., Li, X., Liu, Y., Wang, Y., Guo, H., Hou, J., Zhu, T., Liu, Y., 2023a. Net-zero greenhouse gas emission from wastewater treatment: mechanisms, opportunities and perspectives. Renew. Sustain. Energy Rev. 184, 113547.
He, Y., Liu, Y., Li, X., Guo, H., Zhu, T., Liu, Y., 2024. Polyvinyl chloride microplastics facilitate nitrous oxide production in partial nitritation systems. Environ. Sci. Technol. 58 (4), 1954–1965.
He, Y., Liu, Y., Li, X., Zhu, T., Liu, Y., 2023b. Unveiling the roles of biofilm in reducing N2O emission in a nitrifying integrated fixed-film activated sludge (IFAS) system. Water Res. 243, 120326.
He, Y., Liu, Y., Yan, M., Zhao, T., Liu, Y., Zhu, T., Ni, B.-J., 2022. Insights into N2O turnovers under polyethylene terephthalate microplastics stress in mainstream biological nitrogen removal process. Water Res. 224, 119037.
Jachimowicz, P., Jo, Y.-J., Cydzik-Kwiatkowska, A., 2022. Polyethylene microplastics increase extracellular polymeric substances production in aerobic granular sludge. Sci. Total Environ. 851, 158208.
Li, L., Li, F., Deng, M., Wu, C., Zhao, X., Song, K., Wu, F., 2022. Microplastics distribution characteristics in typical inflow rivers of Taihu lake: linking to nitrous oxide emission and microbial analysis. Water Res. 225, 119117.
Li, L., Song, K., Yeerken, S., Geng, S., Liu, D., Dai, Z., Xie, F., Zhou, X., Wang, Q., 2020. Effect evaluation of microplastics on activated sludge nitrification and denitrification. Sci. Total Environ. 707, 135953.
Li, X., Gao, D., Li, Y., Zheng, Y., Dong, H., Liang, X., Liu, M., Hou, L., 2023. Increased nitrogen loading facilitates nitrous oxide production through fungal and chemodenitrification in estuarine and coastal sediments. Environ. Sci. Technol. 57 (6), 2660–2671.
Liu, C., Guo, Z., Zhang, H., Li, J., Zhu, C., Zhu, G., 2023a. Single-cell Raman spectra reveals the cytochrome c-mediated electron transfer in nanoscale zero-valent iron coupled denitrification process. Chem. Engineer. J. 454, 140241.
Liu, S., Guo, H., Wang, Y., Hou, J., Zhu, T., Liu, Y., 2023b. Peracetic acid activated by ferrous ion mitigates sulfide and methane production in rising main sewers. Water Res. 245, 120584.
Liu, Y., He, Y., Chen, F., Ren, S., Zhao, T., Zhu, T., Liu, Y., 2023c. Flocs enhance nitrous oxide reduction capacity in a denitrifying biofilm-based system: mechanism of electron competition. Chem. Engineer. J. 455, 140599.
Liu, Y., Liu, Y., Zhao, T., He, Y., Zhu, T., Chai, H., Peng, L., 2024. Smaller aerobic granules significantly reduce N2O production by ammonia-oxidizing bacteria: evidences from biochemical and isotopic analyses. Environ. Sci. Technol. 58 (1), 545–556.
Mahon, A.M., O'Connell, B., Healy, M.G., O'Connor, I., Officer, R., Nash, R., Morrison, L., 2017. Microplastics in sewage sludge: effects of treatment. Environ. Sci. Technol. 51 (2), 810–818.
Mintenig, S.M., Int-Veen, I., Löder, M.G.J., Primpke, S., Gerdts, G., 2017. Identification of microplastic in effluents of waste water treatment plants using focal plane array-based micro-Fourier-transform infrared imaging. Water Res. 108, 365–372.
Oberoi, A.S., Huang, H., Khanal, S.K., Sun, L., Lu, H., 2021. Electron distribution in sulfur-driven autotrophic denitrification under different electron donor and acceptor feeding schemes. Chem. Engineer. J. 404, 126486.
Pan, Y., Ni, B.-J., Bond, P.L., Ye, L., Yuan, Z., 2013a. Electron competition among nitrogen oxides reduction during methanol-utilizing denitrification in wastewater treatment. Water Res. 47 (10), 3273–3281.
Pan, Y., Ni, B.-J., Yuan, Z., 2013b. Modeling electron competition among nitrogen oxides reduction and N2O accumulation in denitrification. Environ. Sci. Technol. 47 (19), 11083–11091.
Peng, L., Ni, B.-J., Ye, L., Yuan, Z., 2015. The combined effect of dissolved oxygen and nitrite on N2O production by ammonia oxidizing bacteria in an enriched nitrifying sludge. Water Res. 73, 29–36.
Qi, Y., Armbruster, U., Schmitz-Linneweber, C., Delannoy, E., Longevialle, A.F.D., Rühle, T., Small, I., Jahns, P., Leister, D., 2012. Arabidopsis CSP41 proteins form multimeric complexes that bind and stabilize distinct plastid transcripts. J. Exp. Bot. 63 (3).
Qin, R., Su, C., Liu, W., Tang, L., Li, X., Deng, X., Wang, A., Chen, Z., 2020. Effects of exposure to polyether sulfone microplastic on the nitrifying process and microbial community structure in aerobic granular sludge. Bioresour. Technol. 302, 122827.
Sazanov, L.A., Hinchliffe, P., 2006. Structure of the hydrophilic domain of respiratory complex I from *Thermus thermophilus*. Science (1979) 311 (5766), 1430–1436.
Seeley, M.E., Song, B., Passie, R., Hale, R.C., 2020. Microplastics affect sedimentary microbial communities and nitrogen cycling. Nat. Commun. 11 (1), 2372.
Shi, X., Shi, R., Fu, X., Zhao, Y., Ge, Y., Liu, J., Chen, C., Liu, W., 2024. Impact of microplastics on plant physiology: a meta-analysis of dose, particle size, and crop type interactions in agricultural ecosystems. Sci. Total Environ. 955, 177245.
Su, Z., Liu, T., Guo, J., 2023. Nitrite oxidation in wastewater treatment: microbial adaptation and suppression challenges. Environ. Sci. Technol. 57 (34), 12557–12570.
Tian, L., Guo, H., Wang, Y., Wang, X., Zhu, T., Liu, Y., 2022. Urine source separation-based pretreatment: a sustainable strategy for improving methane production from anaerobic digestion of waste activated sludge. Sustainable Horizons 4, 100043.
Tong, Y., Liao, X., He, Y., Cui, X., Wishart, M., Zhao, F., Liao, Y., Zhao, Y., Lv, X., Xie, J., Liu, Y., Chen, G., Hou, L.a., 2024. Mitigating greenhouse gas emissions from municipal wastewater treatment in China. Environ. Sci. Ecotechnol. 20, 100341.
Vieira, A., Galinha, C.F., Oehmen, A., Carvalho, G., 2019. The link between nitrous oxide emissions, microbial community profile and function from three full-scale WWTPs. Sci. Total Environ. 651, 2460–2472.

Wang, Y., Chen, F., Guo, H., Sun, P., Zhu, T., Horn, H., Liu, Y., 2024a. Permanganate (PM) pretreatment improves medium-chain fatty acids production from sewage sludge: the role of PM oxidation and in-situ formed manganese dioxide. Water Res. 249, 120869.
Wang, Y., Guo, H., Li, X., Chen, X., Peng, L., Zhu, T., Sun, P., Liu, Y., 2024b. Peracetic acid (PAA)-based pretreatment effectively improves medium-chain fatty acids (MCFAs) production from sewage sludge. Environ. Sci. Ecotechnol. 20, 100355.
Wang, Y., Sun, P., Guo, H., Zheng, K., Zhu, T., Liu, Y., 2022. Performance and mechanism of sodium percarbonate (SPC) enhancing short-chain fatty acids production from anaerobic waste activated sludge fermentation. J. Environ. Manage. 313, 115025.
Wang, Y., Zheng, K., Guo, H., Tian, L., He, Y., Wang, X., Zhu, T., Sun, P., Liu, Y., 2023. Potassium permanganate-based advanced oxidation processes for wastewater decontamination and sludge treatment: a review. Chem. Engineer. J. 452, 139529.
Wang, Z., Gao, J., Dai, H., Zhao, Y., Li, D., Duan, W., Guo, Y., 2021. Microplastics affect the ammonia oxidation performance of aerobic granular sludge and enrich the intracellular and extracellular antibiotic resistance genes. J. Hazard. Mater. 409, 124981.
Wei, W., Hao, Q., Chen, Z., Bao, T., Ni, B.-J., 2020. Polystyrene nanoplastics reshape the anaerobic granular sludge for recovering methane from wastewater. Water Res. 182, 116041.
Xi, Z., Guo, J., Lian, J., Li, H., Zhao, L., Liu, X., Zhang, C., Yang, J., 2013. Study the catalyzing mechanism of dissolved redox mediators on bio-denitrification by metabolic inhibitors. Bioresour. Technol. 140, 22–27.
Xiang, Y., Zhou, T., Deng, S., Shao, Z., Liu, Y., He, Q., Chai, H., 2023. Nitrite improved nitrification efficiency and enriched ammonia-oxidizing archaea and bacteria in the simultaneous nitrification and denitrification process. Water. Res. X. 21, 100204.
Yang, L., Li, K., Cui, S., Kang, Y., An, L., Lei, K., 2019. Removal of microplastics in municipal sewage from China's largest water reclamation plant. Water Res. 155, 175–181.
Yu, X.-L., Zhao, Z.-T., Zhao, H.-B., He, S.-S., Cui, C.-H., Sun, H.-J., Zhao, Y.-L., Bai, S.-W., Dong, J., Pang, J.-W., Ding, J., Ren, N.-Q., Yang, S.-S., 2022. Mapping research on carbon neutrality in WWTPs between 2001 and 2021: a scientometric and visualization analysis. Sustain. Horizons 3, 100022.
Zhang, B., Xu, X., Zhu, L., 2017. Structure and function of the microbial consortia of activated sludge in typical municipal wastewater treatment plants in winter. Sci. Rep. 7 (1), 17930.
Zhang, J., Chen, Z., Liu, Y., Wei, W., Ni, B.-J., 2024a. Removal of emerging contaminants (ECs) from aqueous solutions by modified biochar: a review. Chem. Engineer. J. 479, 147615.
Zhang, W., Liu, X., Liu, L., Lu, H., Wang, L., Tang, J., 2022. Effects of microplastics on greenhouse gas emissions and microbial communities in sediment of freshwater systems. J. Hazard. Mater. 435, 129030.
Zhang, Y.-T., Wei, W., Huang, Q.-S., Wang, C., Wang, Y., Ni, B.-J., 2020. Insights into the microbial response of anaerobic granular sludge during long-term exposure to polyethylene terephthalate microplastics. Water Res. 179, 115898.
Zhang, Z., Wang, Y., Wang, X., Zhang, Y., Zhu, T., Peng, L., Xu, Y., Chen, X., Wang, D., Ni, B.-J., Liu, Y., 2024b. Towards scaling-up implementation of polyhydroxyalkanoate (PHA) production from activated sludge: progress and challenges. J. Clean. Prod. 447, 141542.
Zheng, M., Hu, Z., Liu, T., Sperandio, M., Volcke, E.I.P., Wang, Z., Hao, X., Duan, H., Vlaeminck, S.E., Xu, K., Zuo, Z., Guo, J., Huang, X., Daigger, G.T., Verstraete, W., van Loosdrecht, M.C.M., Yuan, Z., 2024. Pathways to advanced resource recovery from sewage. Nat. Sustain. 7 (11), 1395–1404.
Zheng, M., Li, H., Duan, H., Liu, T., Wang, Z., Zhao, J., Hu, Z., Watts, S., Meng, J., Liu, P., Rattier, M., Larsen, E., Guo, J., Dwyer, J., Akker, B.V.D., Lloyd, J., Hu, S., Yuan, Z., 2023. One-year stable pilot-scale operation demonstrates high flexibility of mainstream anammox application. Water. Res. X. 19, 100166.
Zheng, X., Han, Z., Shao, X., Zhao, Z., Zhang, H., Lin, T., Yang, S., Zhou, C., 2022. Response of aerobic granular sludge under polyethylene microplastics stress: physicochemical properties, decontamination performance, and microbial community. J. Environ. Manage. 323, 116215.
Ziajahromi, S., Neale, P.A., Rintoul, L., Leusch, F.D.L., 2017. Wastewater treatment plants as a pathway for microplastics: development of a new approach to sample wastewater-based microplastics. Water Res. 112, 93–99.